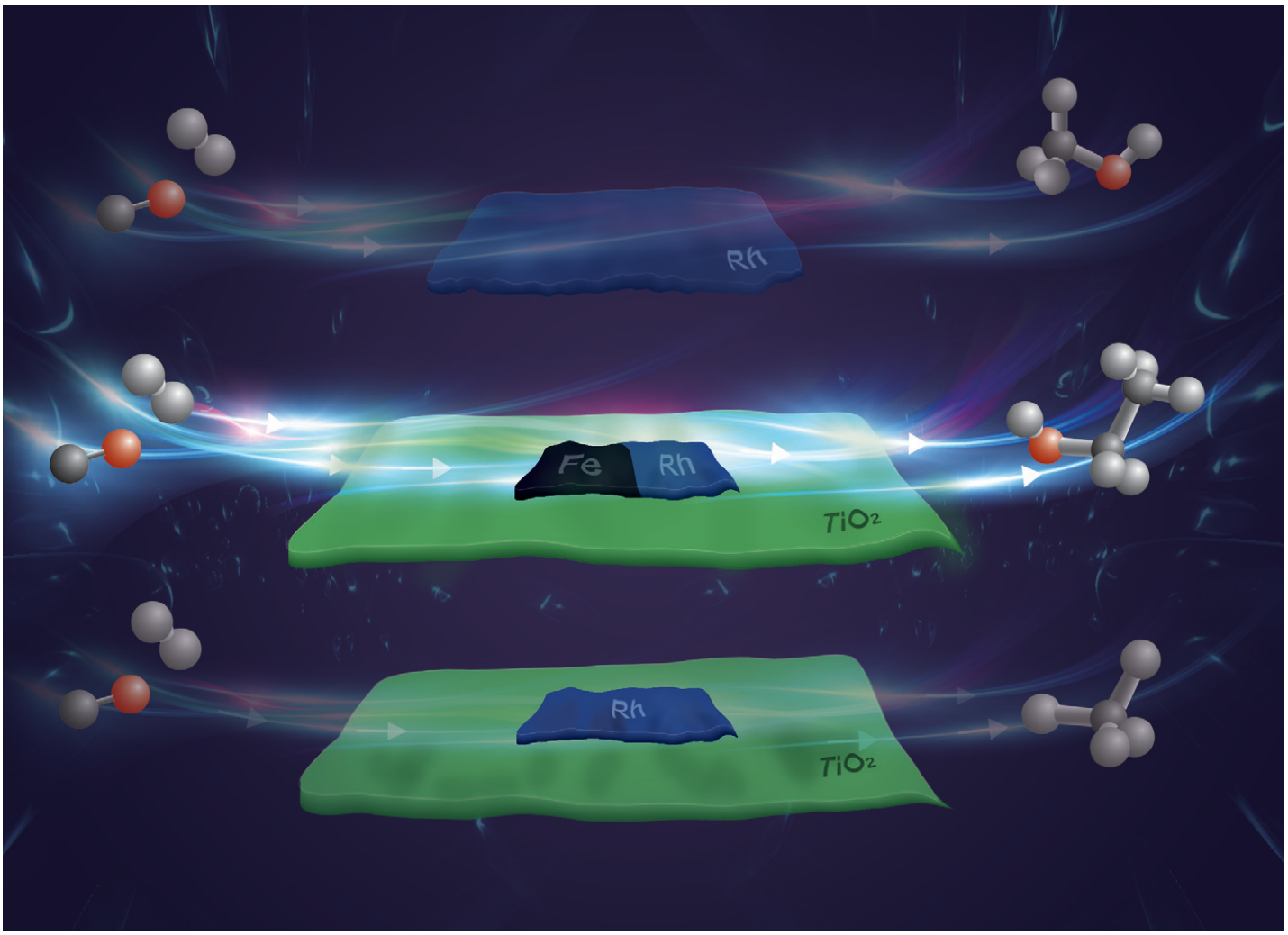

Showcasing research from Prof. Baojun Wang's group at Taiyuan University of Technology, China.

Catalytic selectivity of Rh/TiO_2 catalyst in syngas conversion to ethanol: probing into the mechanism and functions of TiO_2 support and promoter

In order to achieve high ethanol productivity and selectivity, an effective Rh-based catalyst must be a suitable combination of supports and promoters, in which the promoter M should have characteristics that make the d-band center of the MRh/TiO_2 catalyst closer to the Fermi level.

As featured in:

See Baojun Wang *et al.*, *Catal. Sci. Technol.*, 2017, **7**, 1073.

ROYAL SOCIETY OF CHEMISTRY

rsc.li/catalysis

Registered charity number: 207890

Catalysis Science & Technology

PAPER

Cite this: *Catal. Sci. Technol.*, 2017, 7, 1073

Catalytic selectivity of Rh/TiO_2 catalyst in syngas conversion to ethanol: probing into the mechanism and functions of TiO_2 support and promoter†

Riguang Zhang, Mao Peng and Baojun Wang*

Received 9th November 2016,
Accepted 2nd January 2017

DOI: 10.1039/c6cy02350a

rsc.li/catalysis

The catalytic selectivity, the functions of a TiO_2 support and promoter, and the mechanism of ethanol synthesis from syngas on a Rh/TiO_2 model catalyst have been fully identified. Our results show that all species preferentially interact with Rh_7 clusters of a Rh/TiO_2 catalyst, rather than the support and cluster–support interface. CO → CHO → CH_2O → CH_3O is an optimal pathway. CH_3 formed *via* the CH_3O → CH_3 + O route is the most favored CH_x (x = 1–3) monomer, and this route is more favorable than methanol formation by CH_3O hydrogenation; CO insertion into CH_3 can then form CH_3CO, followed by successive hydrogenation to ethanol. Methane is formed by CH_3 hydrogenation. The Rh/TiO_2 catalyst exhibits better catalytic activity and selectivity toward CH_3 than CH_3OH formation. Starting from the CH_3 species, CH_4 formation is more favorable than CH_3CO formation; thus, ethanol productivity and selectivity on a Rh/TiO_2 catalyst with a support is determined only by CH_4 formation, which is similar to that on a pure Rh catalyst without a support. Introducing an Fe promoter into the Rh/TiO_2 catalyst effectively suppresses methane production, and promotes CH_3CO formation. Therefore, compared to a pure Rh catalyst without a support, the TiO_2 support serves only to promote the activity and selectivity of CH_3 formation, and provide more CH_3 species for ethanol formation; methane formation is independent of the Rh catalyst support, and depends only on the promoter. In order to achieve high ethanol productivity and selectivity, an effective Rh-based catalyst must contain a suitable combination of supports and promoters, in which the promoter, M, should have characteristics that draw the d-band center of the MRh/TiO_2 catalyst closer to the Fermi level compared to the Rh_7/TiO_2 catalyst; as a result, the MRh/TiO_2 catalyst can suppress CH_4 production and facilitate C_2 oxygenate formation.

1. Introduction

Ethanol formation from syngas is a major industrial process, since syngas can be conveniently obtained from natural gas, coal and biomass.[1] Ethanol formation from syngas was first patented by the Union Carbide Corporation using a Rh catalyst;[2] however, the Rh component alone exhibits poor activity, and mainly results in hydrocarbon products, together with methanol as the primary oxygenate; thus, in order to achieve high ethanol productivity and selectivity, extensive efforts have been focused on Rh-based catalysts in order to improve the dispersion of Rh and to modify Rh using promoters and/or supports.[3–6] Up to now, Rh-based catalysts have been widely studied with respect to ethanol formation from syngas,[1,7–17] and are one of the better groups of materials that convert syngas directly into ethanol, rather than *via* methanol.[1,12,18] Furthermore, ethanol formation from syngas generally involves several key steps, including CO dissociation and hydrogenation to form CH_x species, and CO/CHO insertion into CH_x to form C_2 oxygenates, followed by successive hydrogenation to ethanol.[19–21] Modifications using promoters and/or supports usually promote one or more of these key steps; as a result, syngas can be efficiently converted to the desired products.[17] So far, several experimental studies on promoters and supports that contribute to higher activity and selectivity toward C_2 oxygenates have been reported. The addition of

Key Laboratory of Coal Science and Technology of Ministry of Education and Shanxi Province, Taiyuan University of Technology, Taiyuan 030024, Shanxi, P.R. China. E-mail: quantumtyut@126.com, wangbaojun@tyut.edu.cn; Fax: +86 351 6041237; Tel: +86 351 6018239

† Electronic supplementary information (ESI) available: Descriptions of the structures of Rh heptamer clusters (part 1), the reactions related to CH and CH_2 species (part 2), the calculation of the rate constants (part 3) and microkinetic modeling (part 4), the reactions of CH_3 + CO → CH_3CO and CH_3 + H → CH_4 on the Fe-promoted Rh/TiO_2 catalyst (part 5), densities of states of Rh_7/TiO_2 and $FeRh_6/TiO_2$ catalysts, and the corresponding adsorbed species in CH_3 hydrogenation and CO insertion into CH_3 (part 6) have been presented in detail. See DOI: 10.1039/c6cy02350a

promoters, such as Fe, Mn, Li, Ti, La, Sm, and V, could notably increase the activity and selectivity toward target products,[13,22–27] suggesting that these present a strong ability to suppress CH_x hydrogenation, which not only decreases hydrocarbon selectivity, but also promotes C_2 oxygenate selectivity.

On the other hand, it is well known that supported Rh-based catalysts exhibit excellent performances in the synthesis of C_2 oxygenates, such as ethanol and acetaldehyde, from syngas,[7,28–30] in which the support presents the functions of dispersing metal particles and modifying the properties of active metal species through metal–support interactions.[17] Meanwhile, previous studies have shown that the selectivity of CO hydrogenation depends closely on the chemical nature of the supports;[31–33] for example, Rh supported on strongly basic oxides, such as MgO and ZnO, yielded methanol as a major product,[31] whereas Rh supported on oxides, such as SiO_2 and Al_2O_3, favored methane and higher hydrocarbons as the major products;[32] however, Rh supported on TiO_2 gave the highest ethanol selectivity.[33] Erdöhelyi and Solymosi[34] reported that among TiO_2, Al_2O_3, SiO_2, and MgO-supported Rh catalysts, a TiO_2-supported Rh catalyst exhibited the highest selectivity to ethanol from syngas; Haider *et al.*[13] found that negligible ethanol was produced over 2 wt% Rh on a SiO_2 support, while a similar loading of Rh on a TiO_2 support was active for ethanol formation from syngas. Finally, it has been reported that Ti as a promoter or as a support could promote C_2 oxygenate formation.[23,24,34,35] As a result, many studies focused on TiO_2-supported Rh-based catalysts with excellent performances for ethanol synthesis from syngas;[15,36–38] however, the underlying mechanism and the function of the supports in improving the catalytic activity and selectivity for ethanol synthesis from syngas remain unclear.

Nowadays, theoretical calculations have been used as a powerful tool to elucidate the mechanism of several typical reactions;[18,39–51] for example, density functional theory (DFT) calculations by Choi and Liu[18] have indicated that ethanol selectivity from syngas on a periodic Rh(111) surface without a support largely depends on the relative activity of CH_3 hydrogenation to CH_4 compared to CO insertion into CH_3 to form CH_3CO. Shetty *et al.*[52] have investigated C_1 and C_2 oxygenate formation from syngas over a pure Rh_6 cluster, indicating that C_1 oxygenates are formed *via* CO hydrogenation, while C_2 oxygenate formation proceeds *via* CO dissociation to produce CH_x species, followed by CO and/or CHO insertion. However, few theoretical studies on Rh-based catalysts modified by a support have been carried out to fully understand the function of the support and the underlying mechanism of ethanol synthesis from syngas at the molecular level, due to the complexity of the reactions. As a result, we cannot obtain the intrinsic information required to fabricate a more effective Rh-based catalyst in a real catalytic system; thus, this motivates us to probe into the specific role of the support.

In this study, the functions of the support and promoter, the catalytic selectivity, and the mechanism of ethanol synthesis from syngas over TiO_2-supported Rh-based catalysts have been clarified by DFT calculations and microkinetic modeling, together with a cluster/support model catalyst. By probing into the mechanism of ethanol synthesis from syngas, we can obtain a clear picture of ethanol formation on TiO_2-supported Rh catalysts; the results are expected to readdress the following questions: what are the functions of the support and the promoter? What is the productivity and selectivity-controlling step of ethanol formation? Why are the support and promoter needed to achieve high ethanol productivity and selectivity? How do our results for the model systems bridge the gap between the computational and the real experimental system? Furthermore, a detailed mechanistic investigation of ethanol synthesis from syngas over TiO_2-supported Rh-based catalysts at the molecular level will not only help us to better understand the underlying mechanism, but will also serve as a basis for the selective modification of Rh-based catalysts to improve the catalytic selectivity toward the desired products.

2. Computational details

2.1. Computational models

The TiO_2 support, widely used in catalysis,[53–60] exists in the form of three polymorphs: rutile, anatase, and brookite; among them, the rutile form is the most common polymorph of TiO_2, and is the most thermodynamically stable form at ordinary pressures and temperatures up to its melting point, 1830 K.[61] Among the low-index faces naturally presented in the rutile form, the (110) face is the most stable one;[62–64] as a result, many theoretical and experimental studies have used the rutile (110) face as a model surface.[53,65–68] In this study, the rutile (110) surface is modeled using a $p(3 \times 2)$ unit cell slab with 9 atomic layers,[69–73] and a 15 Å vacuum space along the *z*-direction is employed to prevent interactions between any two successive slabs.

Previous experimental studies[74–76] have shown that a supported Rh cluster has alternating (100) and (111) crystal facets; EXAFS[77–79] and STM[77,80] have shown that a supported Rh cluster has an average particle height of 0.4–0.5 nm. Recently, Guan *et al.*[81] prepared a sub-nano Rh/TiO_2 catalyst with Rh clusters having a specific size range of 0.4–0.8 nm. Here, we attempt to present a representative model that includes the physical properties mentioned above under realistic conditions. On the basis of these studies, we focus on a Rh_7 cluster with 7 Rh atoms for our supported Rh cluster model.

For the Rh_7 cluster model, eleven possible structures have been considered (see Fig. S1†),[82] indicating that both the coupled tetragonal pyramid (CTP) and the capped octahedron (COh) are the most stable structures (see Fig. 1(a) and (b), respectively);[83,84] both the CTP and COh structures have an particle height near 0.4 nm within the size distribution mentioned in the above experiments.[77–81] Furthermore, when a Rh_7 cluster with a CTP or a COh

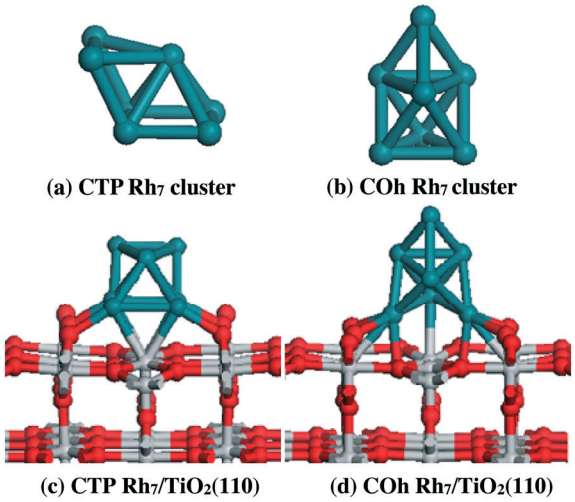

Fig. 1 The most stable configurations of Rh_7 clusters and the oxide-supported $Rh_7/TiO_2(110)$, (a) CPT Rh_7 cluster, (b) COh Rh_7 cluster, (c) CPT Rh_7 cluster/$TiO_2(110)$, and (d) COh Rh_7 cluster/$TiO_2(110)$. O, Ti and Rh atoms are shown by red, grey, and dark cyan balls, respectively.

structure is supported over a $TiO_2(110)$ surface, the most stable configurations of the cluster–support are obtained, as presented in Fig. 1(c) and (d), respectively, suggesting that a CTP structure adsorbed on a $TiO_2(110)$ surface has much stronger metal–support interactions than a COh structure adsorbed on a $TiO_2(110)$ surface (609.2 *vs.* 522.6 kJ mol^{-1}).

Therefore, in this study, the most stable configuration of a Rh_7 cluster with a CTP structure adsorbed on a $p(3 \times 2)$ $TiO_2(110)$ surface ($Rh_7/TiO_2(110)$) is selected as a Rh/TiO_2 model catalyst, as shown in Fig. 1(c); moreover, a Rh_7 cluster with a CTP structure has the characteristics of a 4-fold hollow with a (100) facet and a 3-fold hollow site with a (111) facet, as observed experimentally.[74–76] In addition, since this study mainly focuses on qualitatively understanding the function of a support in a Rh/TiO_2 catalyst, by comparison with a pure Rh catalyst without a support, we think that the $Rh_7/TiO_2(110)$ model catalyst can qualitatively reflect the particle size and structural characteristics of a Rh/TiO_2 catalyst under realistic conditions; further details about the particle model have not been considered.

On the other hand, TiO_2 may be hydroxylated, reduced, or reconstructed under realistic conditions; this study only focuses on ideal TiO_2 to probe into the role of the support rather than the support surface properties; however, the obtained results can provide a fundamental understanding and method for a hydroxylated, reduced, or reconstructed TiO_2 support, which will be considered in a further study. Meanwhile, a realistic catalyst might have differences from the model situation considered in these DFT calculations. It is clear that these calculations are very demanding, and that one has to make severe simplifications in the structural model and the choice of surface structure. Thus, this study can only give a qualitative understanding of what might and might not be important in view of the limitations of the simple $Rh_7/TiO_2(110)$ model catalyst.

2.2. Calculation methods

All DFT calculations are performed by using the Vienna *Ab Initio* Simulation Package (VASP).[85–87] The generalized gradient approximation (GGA) with the Perdew–Wang formulation (PW91) is adopted for the exchange–correlation function.[88] The electron–ion interaction is modeled by the projected-augmented wave (PAW) method.[89] Spin-polarization is included in all structures presented here. The Brillouin zone is sampled using a $2 \times 2 \times 1$ Monkhorst–Pack *k*-point grid[90] with Methfessel-Paxton smearing of 0.2 eV.[91] The plane-wave cutoff energy is set at 400 eV to describe the electronic wave functions. A force difference between two steps of less than 0.05 eV $Å^{-1}$ is used as the criterion for convergence of ionic relaxation. The relaxation of the electronic degrees of freedom is assumed to be converged, if the total energy change and the band structure energy change between two steps are both smaller than 1×10^{-5} eV. To better describe on-site Coulomb interactions, a DFT + *U* method is used with a suggested *U* value of 4.0 eV.[92,93]

Reaction pathways have been investigated using the climbing-image nudged elastic band method (CI-NEB).[94,95] Transition states have been optimized using the dimer method.[96,97] The structure of a transition state is deemed to be converged when the forces acting on the atoms are all <0.05 eV $Å^{-1}$ for the various degrees of freedom set in the calculation. The molecules in the gas phase are calculated using a $10 \times 10 \times 10$ Å cubic unit cell. During the calculations, the upper six layers of the $TiO_2(110)$ surface, together with the adsorbed species and Rh_7 cluster, are relaxed, whereas the bottom three layers of the $TiO_2(110)$ surface are fixed at their bulk positions. All transition states are confirmed with only one imaginary frequency.

In ethanol synthesis from syngas, the adsorption of reactants, intermediates and products is firstly investigated over the Rh/TiO_2 catalyst; then, the formation mechanisms of CH_x (x = 1–3) species, C_2 oxygenates, and ethanol are examined; furthermore, the differences in ethanol synthesis over Rh/TiO_2 with a support and the pure Rh catalyst without a support are identified to determine the role of the support. In addition, in order to understand the reaction mechanism, only one or two adsorbates are presented on the Rh/TiO_2 catalyst in this study; the effect of other adsorbates on the reaction has not been considered.

3. Results and discussion

3.1. Adsorption of all possible species in ethanol synthesis

For the adsorption of the species involved in ethanol formation over the Rh/TiO_2 catalyst, all possible adsorption sites over Rh_7 clusters and Rh_7 cluster–TiO_2 support interfaces have been examined. Fig. S2† presents the most stable configurations of these species and the corresponding adsorption energies. The results suggest that all species preferentially adsorb at the Rh_7 cluster rather than the support and cluster–support interfaces; namely, the Rh_7 cluster over the

Rh/TiO_2 catalyst is the active composition for catalyzing ethanol synthesis.

3.2. CH_x (x = 1–3) formation

CH_x (x = 1–3) species are a key issue in ethanol synthesis from syngas. Two possibilities exist for CH_x (x = 1–3) formation: one is direct dissociation of CO to C, followed by C hydrogenation to form CH_x (x = 1–3) species; the other is CO hydrogenation to CH_xO or CH_xOH intermediates, followed by H-assisted or non-H-assisted C–O bond scission to form CH_x (x = 1–3). Table 1 lists the activation energies and reaction energies of all the elementary reactions involved in ethanol synthesis.

On the other hand, our previous studies[98] have shown that the adsorption of H_2 with different coverages on Rh surfaces is dissociative adsorption with the dissociative H atoms adsorbed on the Rh surface, suggesting that H_2 predominantly exists in the form of H atoms on the Rh catalyst under realistic conditions. Therefore, in this study, only the interactions of H atoms have been considered, rather than those of H_2 molecules.

Table 1 The elementary reactions involved in ethanol synthesis from syngas, together with the corresponding activation energies (E_a) and reaction energies (ΔH)

	Elementary reactions	Transition state	E_a/kJ mol^{-1}	ΔH/kJ mol^{-1}
(R1)	CO → C + O	TS1	340.0	180.7
(R2)	CO + H → CHO	TS2	56.0	3.7
(R3)	CO + H → COH	TS3	117.6	0.7
(R4)	CHO → CH + O	TS4	227.3	57.9
(R5)	CHO + H → CH + OH	TS5	216.5	30.8
(R6)	CHO + H → CHOH	TS6	122.6	39.6
(R7)	CHOH → CH + OH	TS7	96.6	−8.8
(R8)	CHOH + H → CH + H_2O	TS8	67.9	−68.8
(R9)	CHO + H → CH_2O	TS9	20.8	−25.5
(R10)	CHO + H → CH_2 + O	TS10	145.0	13.6
(R11)	CH_2O → CH_2 + O	TS11	171.8	39.1
(R12)	CH_2O + H → CH_2 + OH	TS12	170.6	28.8
(R13)	CH_2O + H → CH_2OH	TS13	126.7	18.2
(R14)	CH_2OH → CH_2 + OH	TS14	74.2	10.6
(R15)	CH_2OH + H → CH_2 + H_2O	TS15	37.5	−26.5
(R16)	CH_2O + H → CH_3O	TS16	50.6	19.6
(R17)	CH_2O + H → CH_3 + O	TS17	147.6	−8.6
(R18)	CH_3O → CH_3 + O	TS18	87.4	−28.2
(R19)	CH_3O + H → CH_3 + OH	TS19	138.8	−67.5
(R20)	CH_3O + H → CH_3OH	TS20	95.6	−52.1
(R21)	CH_3 + CO → CH_3CO	TS21	108.7	62.6
(R22)	CH_3 + CHO → CH_3CHO	TS22	83.1	5.5
(R23)	CH_3 → CH_2 + H	TS23	35.3	11.2
(R24)	CH_3 + H → CH_4	TS24	72.4	42.8
(R25)	CH_3 + CH_3 → C_2H_6	TS25	119.7	−46.1
(R26)	CH_2 + CO → CH_2CO	TS26	101.2	64.1
(R27)	CH_2 + CHO → CH_2CHO	TS27	80.3	−11.7
(R28)	CH_2 → CH + H	TS28	40.1	26.6
(R29)	CH_2 + H → CH_3	TS29	24.1	−11.2
(R30)	CH_2 + CH_2 → C_2H_4	TS30	178.2	−4.7
(R31)	CH + CO → CHCO	TS31	169.0	91.6
(R32)	CH + CHO → CHCHO	TS32	128.7	11.4
(R33)	CH → C + H	TS33	98.6	−181.5
(R34)	CH + H → CH_2	TS34	13.5	−26.6
(R35)	CH + CH → C_2H_2	TS35	78.3	−125.7
(R36)	CH_3CO + H → CH_3CHO	TS36	85.2	44.4
(R37)	CH_3CO + H → CH_3COH	TS37	114.1	35.9
(R38)	CH_3CHO + H → CH_3CH_2O	TS38	78.4	−10.9
(R39)	CH_3CHO + H → CH_3CHOH	TS39	129.8	43.2
(R40)	CH_3CH_2O + H → C_2H_5OH	TS40	95.8	17.8

3.2.1. Initial CO step. For the initial CO step, as shown in Table 1 and Fig. S3,† three reactions (**R1**–**R3**) may occur. CHO formation, with an activation energy and a reaction energy of 56.0 and 3.7 kJ mol^{-1}, respectively, is more favorable kinetically than COH formation and direct CO dissociation. Thus, CHO is the predominant product of the initial CO step over the Rh/TiO_2 catalyst. Moreover, experiments have also confirmed the significance of CHO species in alcohol synthesis on a Rh/SiO_2 catalyst;[99] meanwhile, on a Rh_6 cluster without a support,[52] as well as on periodic Rh(111) and Rh(211) surfaces,[18,84] CO hydrogenation to CHO is also the most favorable pathway.

3.2.2. CH formation. As mentioned above, CHO is the predominant product of the initial CO step over the Rh/TiO_2 catalyst. Thus, starting from the CHO species, CH can be produced from CHO and a CHOH intermediate (see **R4**, **R5**, **R7**, and **R8** in Table 1); meanwhile, CHO hydrogenation to CH_2O (**R9**) is also considered.

As shown in Fig. S4,† with respect to CHO or CHO + H species, among four pathways of CH formation, CHO + 2H → CHOH + H → CH + H_2O (**R6**, **R8**) has an overall activation energy of only 122.6 kJ mol^{-1} with a reaction energy of −29.2 kJ mol^{-1}, which predominantly contributes to CH formation *via* an CHOH intermediate. However, CHO hydrogenation to CH_2O (**R9**) has an activation energy of only 20.8 kJ mol^{-1} with a reaction energy of −25.5 kJ mol^{-1}. Therefore, starting from the CHO species, CHO hydrogenation to CH_2O is the predominant pathway, rather than H-assisted CH formation by CHOH dissociation.

3.2.3. CH_2 formation. The above results show that CHO hydrogenation to CH_2O occurs preferentially on the Rh/TiO_2 catalyst. Thus, starting from CH_2O, CH_2 species can be produced from CH_2O and CH_2OH intermediates (see **R11**, **R12**, **R14**, **R15** in Table 1); meanwhile, H-assisted CHO dissociation can also produce CH_2 species (**R10**); furthermore, CH_2O hydrogenation to CH_3O (**R16**) is also examined.

As shown in Fig. S5,† with respect to CHO + H species, among five pathways of CH_2 formation, the CHO + 3H → CH_2O + 2H → CH_2OH + H → CH_2 + H_2O pathway (**R9**, **R13**, **R15**) has an overall activation energy of only 101.2 kJ mol^{-1} with a reaction energy of −33.8 kJ mol^{-1}, and is predominantly responsible for CH_2 formation *via* the CH_2OH intermediate. However, CH_2O hydrogenation to CH_3O (**R16**) has an activation energy of only 50.6 kJ mol^{-1} with a reaction energy of 19.6 kJ mol^{-1}. Thus, CH_2O hydrogenation to CH_3O is the predominant pathway, rather than H-assisted CH_2 formation by CH_2OH dissociation.

3.2.4. CH_3 formation. Since CH_2O hydrogenation to CH_3O is the main pathway, starting from CH_3O, CH_3 can be formed by direct dissociation of CH_3O and H-assisted CH_3O dissociation (**R18**, **R19**); meanwhile, H-assisted CH_2O dissociation

can also form CH_3 species (**R17**). Furthermore, CH_3OH formation by CH_3O hydrogenation (**R20**) is also considered.

As shown in Fig. S6,† with respect to CHO + H, among three reaction pathways of CH_3 formation, CHO + 2H → CH_2O + H → CH_3O→CH_3 + O (**R9, R16, R18**) has an overall activation energy of only 81.5 kJ mol^{-1} with a reaction energy of −34.1 kJ mol^{-1}, and is predominantly responsible for CH_3 formation. CH_3O hydrogenation to CH_3OH (**R20**) has an overall activation energy of 89.7 kJ mol^{-1} with a reaction energy of −58.0 kJ mol^{-1}. These results indicate that CH_3 formation is favorable than CH_3OH formation with respect to the kinetics.

3.2.5. Brief summary of CH_x (x = 1–3) and CH_3OH formation. With respect to CO + H, Fig. 2 presents the potential energy profile for the most favorable pathway of CH_x (x = 1–3) and CH_3OH formation. CH formation, shown by a black line, has an overall activation energy of 126.3 kJ mol^{-1} with a reaction energy of −25.5 kJ mol^{-1}; the rate-controlling step of this pathway occurs at **TS6**. CH_2 formation, shown by a red line, has an overall activation energy of 104.9 kJ mol^{-1} with a reaction energy of −30.1 kJ mol^{-1}; the rate-controlling step of this pathway occurs at **TS13**. CH_3 formation, shown by a blue line, has an overall activation energy of 85.2 kJ mol^{-1} with a reaction energy of −30.4 kJ mol^{-1}; the rate-controlling step of this pathway occurs at **TS18**. CH_3OH formation, shown by a dark cyan line, has an overall activation energy of 93.4 kJ mol^{-1} with a reaction energy of −54.3 kJ mol^{-1}; the rate-controlling step of this pathway occurs at **TS20**.

On the other hand, comparing the entire process of CH_x formation with that *via* direct CO dissociation, our results show that direct CO dissociation has an activation energy of 340.0 kJ mol^{-1}, which is more than 200 kJ mol^{-1} higher than the overall activation energies of CH_x (x = 1–3) formation and CH_3OH formation.

The above results show that CH_x (x = 1–3) species on the Rh/TiO_2 catalyst predominantly originate from H-assisted CO dissociation *via* CH_xO or CH_xOH intermediates, rather than direct CO dissociation. Moreover, among all the CH_x (x = 1–3) species, CH_3 formation is more favorable than CH and CH_2 formation, both thermodynamically and kinetically; namely, CH_3 is the most favorable monomer formed *via* the process: CO + 3H → CHO + 2H → CH_2O + H → CH_3O → CH_3 + O (**R2, R9, R16, R18**). Meanwhile, CH_3 formation is more favorable than CH_3OH formation with respect to the kinetics, suggesting that the Rh/TiO_2 catalyst can exhibit relatively higher activity and selectivity toward CH_3 formation. Since CH_x is proposed as a prerequisite for C–C chain formation during ethanol synthesis from syngas, the Rh/TiO_2 catalyst provides more CH_3 species for ethanol synthesis.

3.3. The formation of C_2 oxygenates and methane, as well as ethanol

3.3.1. C_2 oxygenates and methane. Previous studies have shown that once the most favorable CH_x monomer is formed, CH_x species are involved in four types of reactions;[41,100] one is CH_x hydrogenation, the second is CH_x coupling to C_2 hydrocarbons, the third is CH_x dissociation, and the fourth is CO or CHO insertion into CH_x to form C_2 oxygenates, which are the key precursors of C_2H_5OH formation.

Since CH_3 is the most favorable monomer among all the CH_x (x = 1–3) species, the potential energy profile of the reactions related to CH_3 species are shown in Fig. 3. Our results show that among all the reactions related to CH_3 species, CH_3 preferentially dissociates to CH_2; the second most favorable reaction is CH_3 hydrogenation to CH_4; the third is CHO insertion into CH_3 to form CH_3CHO; the fourth is CO insertion into CH_3 to form CH_3CO.

As mentioned above, due to easy formation of CH_2 by CH_3 dissociation, all reactions related to CH_2 species (**R26–R30**) have been investigated (see Fig. S7†). Our results show that CH_2 hydrogenation to CH_3 is the most favorable; the second most favorable is CH_2 dissociation to CH; the third is CHO insertion into CH_2 to form CH_2CHO. Furthermore, all

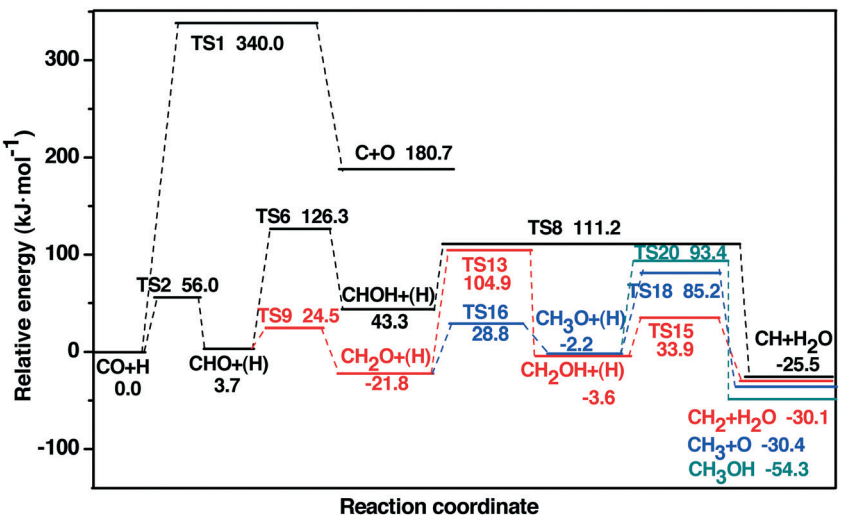

Fig. 2 The potential energy profile for the most favorable routes of CH_x (x = 1–3) and CH_3OH formation.

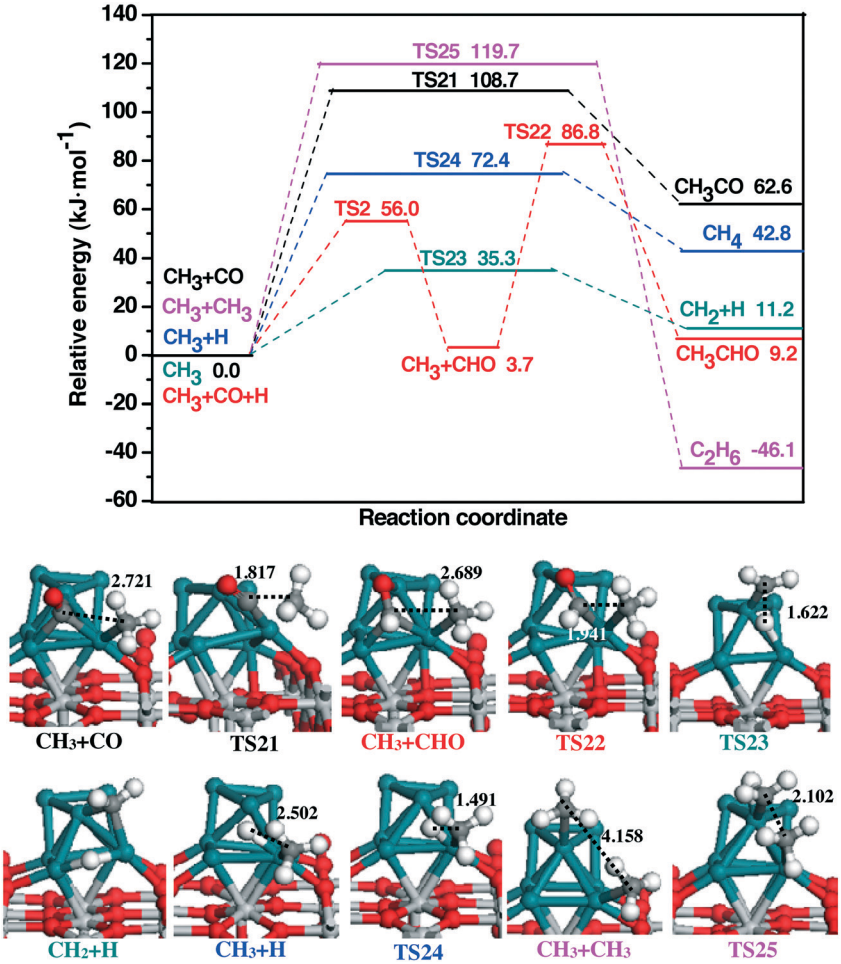

Fig. 3 The potential energy profiles of reactions related to CH_3 species, together with ISs, TSs, and FSs. Bond lengths are in Å. See Fig. S2† for color coding.

reactions related to CH species (**R31–R35**) have also been examined (see Fig. S8†), suggesting that CH is preferentially hydrogenated to CH_2, and the second most favorable is CH coupling, while CHO/CO insertion into CH and CH dissociation occur with difficulty.

The above results show that, starting from CH_3 species, CH and CH_2 can be easily formed by CH_3 dissociation; however, among all reactions related to CH and CH_2 species, CH and CH_2 are preferentially hydrogenated to CH_2 and CH_3, respectively; namely, once CH and CH_2 species are formed, both are preferentially hydrogenated to CH_3. Moreover, previous results[98] have suggested that the saturated coverage of H is 6/12 ML on a Rh catalyst, and the coverage of H_2 can reach 0.3 ML (ref. 101) on a Co catalyst in the presence of 1/3 ML CO in F–T synthesis. As a result, CH and CH_2 species on a Rh/TiO_2 catalyst should be preferentially hydrogenated to CH_3 due to the abundance of hydrogen under realistic conditions. These results further confirm that CH_3 species are the most favorable CH_x monomers on a Rh/TiO_2 catalyst.

For the two insertion pathways that form C_2 oxygenates, our results show that CHO insertion into CH_x (x = 1–3) shows significant superiority to CO insertion into CH_x (x = 1–3) with respect to both thermodynamics and kinetics; this superiority may arise from the smaller HOMO–LUMO gap of CHO compared to that of CO, which facilitates charge transfer and hybridization with a surface.[41,102] Previous studies only compare CO insertion with CHO insertion; however, reactions related to CHO hydrogenation and dissociation have not been compared with CHO insertion. As a matter of fact, starting from CHO species, as well as CHO insertion into CH_x (x = 1–3), CHO can also participate in dissociation reactions to form CO + H and CH + O. Interestingly, our present results show that starting from CHO species, compared to CHO insertion into CH_x (x = 1–3), with activation energies of 128.7, 80.3, and 83.1 kJ mol^{-1}, respectively, CHO hydrogenation to CH_2O only has an activation energy of 20.8 kJ mol^{-1}. Secondly, compared to CHO hydrogenation to CH_2O, CHO dissociation to CO + H or CH + O also has higher activation energies of 52.3 and 227.3 kJ mol^{-1}, respectively. These results show that once CHO is formed, it is hydrogenated to CH_2O in preference to CHO insertion into CH_x (x = 1–3) to form CH_xCHO, or CHO dissociation. Moreover, CHO is predominantly responsible for CH_3 formation by the direct dissociation of CH_3O formed by successive hydrogenations of

CHO *via* CH_2O intermediates. On the other hand, a previous experiment[99] has confirmed the significance of CHO species in alcohol synthesis on Rh/SiO_2 catalysts, and theoretical studies[18,36,82,103] also showed that CHO is predominantly responsible for CH_x formation. Therefore, on the basis of our own and previously reported results, we can show that on a Rh/TiO_2 catalyst, CO insertion into CH_x (x = 1–3) predominantly contributes to the formation of C_2 oxygenates rather than CHO insertion into CH_x (x = 1–3), and CHO is predominantly responsible for the most favored CH_3 monomer production by CHO successive hydrogenations *via* CH_2O intermediates, which provide more CH_3 species for CO insertion to form the ethanol precursor, CH_3CO.

With respect to CH_3 + CO and CH_3 + H species, Fig. 4 presents the potential energy profile for the most favorable formation pathways of C_2 oxygenates and CH_4. The results show that CH_4 formation by CH_3 hydrogenation has an activation energy of 72.4 kJ mol^{-1} with a reaction energy of 42.8 kJ mol^{-1}. Once CH_4 is formed, it does not adhere to the Rh/TiO_2 catalyst and desorbs immediately due to the very small desorption energy of 12.1 kJ mol^{-1} (see Fig. S2†). Alternatively, CO insertion into CH_3 to form CH_3CO has an activation energy of only 108.7 kJ mol^{-1} with a reaction energy of 62.6 kJ mol^{-1}, and is the most favorable pathway among three formation pathways of C_2 oxygenates. On the other hand, CH_2CO is formed by CH_3 dissociation into CH_2, followed by CO insertion; CH_2CO formation has an overall activation energy of 112.4 kJ mol^{-1} with a reaction energy of 75.3 kJ mol^{-1}; however, CH_2 is hydrogenated to CH_3 in preference to insertion of CO among the reactions related to CH_2 species. Moreover, CH_2CO is preferentially hydrogenated to CH_3CO among the reactions related to CH_2CO species.

The above results further confirm that CH_3 is the predominant CH_x (x = 1–3) species, and CO insertion into CH_3 predominantly contributes to the formation of CH_3CO, which is the precursor for ethanol synthesis from syngas on a Rh/TiO_2 catalyst.

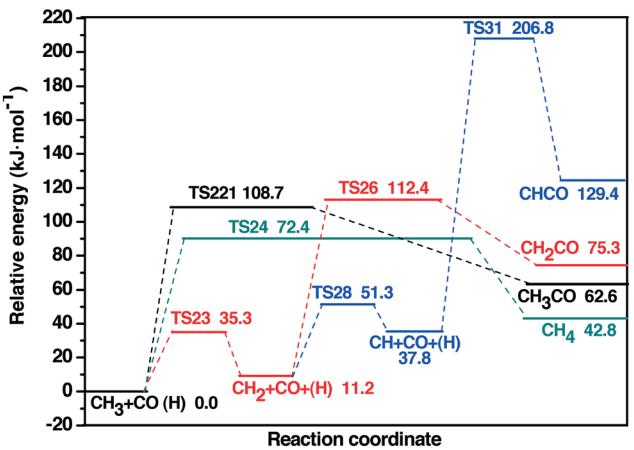

Fig. 4 The potential energy profile for the most favorable formation pathways of C_2 oxygenates and methane with respect to CH_3 + CO species.

3.3.2. Ethanol formation. As mentioned above, CH_3CO is the predominant C_2 oxygenate, and can be hydrogenated to CH_3CHO (**R36**) or CH_3COH (**R37**), as shown in Fig. S9;† CH_3CO hydrogenation to CH_3CHO has an activation energy and a reaction energy of 85.2 and 44.4 kJ mol^{-1}, respectively, and is much more favorable than CH_3COH formation. Meanwhile, CH_3CO has a stronger adsorption energy of 112.8 kJ mol^{-1} over the Rh/TiO_2 catalyst, suggesting that CH_3CO is preferentially hydrogenated to CH_3CHO rather than being desorbed.

Starting from CH_3CHO, CH_3CHO hydrogenation to CH_3CH_2O has an activation energy and a reaction energy of 78.4 and −10.9 kJ mol^{-1}, respectively, and is much more favorable than CH_3CHOH formation, both kinetically and thermodynamically. Meanwhile, CH_3CHO has a stronger adsorption energy of 112.8 kJ mol^{-1} over the Rh/TiO_2 catalyst, suggesting that CH_3CHO is preferentially hydrogenated to CH_3CH_2O rather than being desorbed. Furthermore, CH_3CH_2O hydrogenation to ethanol has an activation energy and a reaction energy of 95.8 and 17.8 kJ mol^{-1}, respectively.

3.4. General discussion

On the basis of the above DFT calculations, it can be found that the adsorption of all species, and all elementary reactions involved in ethanol formation occur at the Rh_7 cluster of the Rh/TiO_2 catalyst, suggesting that the Rh_7 cluster plays a key role in catalyzing syngas conversion. Meanwhile, the optimal formation pathways for ethanol, methane, and methanol have been identified on the Rh/TiO_2 catalyst, as shown in Fig. 5. CO → CHO → CH_2O → CH_3O is an optimal pathway for the initial CO hydrogenation; starting from the CH_3O species, methanol is formed by CH_3O hydrogenation. Ethanol formation firstly involves direct dissociation of CH_3O to CH_3, then, CO insertion into CH_3 can form CH_3CO, followed by

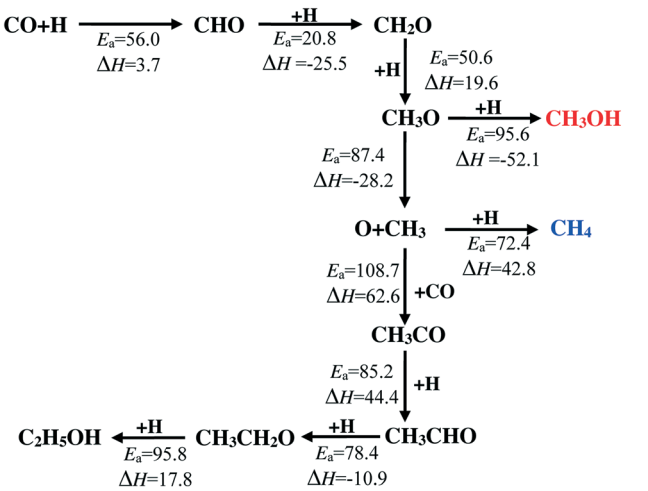

E_a denotes the activation energy for the corresponding step, and ΔH represents the relevant reaction energy (unit: kJ·mol^{-1}).

Fig. 5 Schematic of the most favorable formation pathways of CH_3OH, CH_4, and C_2H_5OH over Rh/TiO_2 model catalyst.

successive hydrogenation to ethanol *via* CH_3CHO and CH_3CH_2O intermediates. Methane is formed by CH_3 hydrogenation.

3.4.1. Microkinetic modeling over Rh/TiO_2 catalyst. With the aim of estimating the formation rates of the major products in ethanol synthesis, microkinetic modeling[18,104–106] has been employed in this study. As mentioned above, for ethanol formation on a Rh/TiO_2 catalyst, the products are expected to be methane, methanol, and ethanol; as a result, the formation rates of methane, methanol, and ethanol, as well as the selectivity for ethanol, will be estimated under typical synthesis conditions. Detailed descriptions of the microkinetic modeling are presented in the ESI.†

Under typical synthesis conditions (p_{CO} = 4 atm, p_{H_2} = 8 atm; T = 500–625 K), on the basis of the microkinetic modeling and the calculated energies in this study, the formation rates and the relative selectivities for CH_4 (r_{CH_4}), CH_3OH (r_{CH_3OH}), and C_2H_5OH ($r_{C_2H_5OH}$) production have been estimated.

The relative selectivities for CH_3OH (r_{CH_3OH}), CH_4 (r_{CH_4}), and C_2H_5OH ($r_{C_2H_5OH}$) production at different temperatures are illustrated in Fig. 6. When the temperature increases, r_{CH_4} decreases from 85.36% to 75.75%, whereas r_{CH_3OH} and $r_{C_2H_5OH}$ increase from 14.62% to 24.18%, and from 0.02% to 0.07%, respectively. Namely, the major product is CH_4, rather than CH_3OH or C_2H_5OH, during syngas conversion on the Rh/TiO_2 catalyst. In addition, based on the reaction network, it is noted that the rate of formation of CH_3 should be equal to those of CH_4 and C_2H_5OH, suggesting that r_{CH_3OH} is much lower than r_{CH_3}, and the major product is CH_3 rather than CH_3OH during CH_x formation from syngas on the Rh/TiO_2 catalyst, and CH_3OH production cannot compete with CH_3 formation.

Microkinetic modeling analysis has also been performed to identify the productivity and selectivity-controlling factors by artificially and independently changing two variables in the kinetic model. The first variable is the activation energy of CO insertion into CH_3 to form CH_3CO; the second variable is the activation energy of CH_3 hydrogenation to CH_4; with the aim of understanding the independent effect of each variable, when one variable is changed, the other is kept the same. As shown in Fig. 7(a), the selectivities of CH_4 and C_2H_5OH are reversed upon lowering the activation energy of CH_3CO formation by only ~30 kJ mol^{-1}; in this way, the selectivity for C_2H_5OH becomes higher than that for CH_4; namely, promoting CH_3CO formation can increase C_2H_5OH production. Alternatively, as shown in Fig. 7(b), a high productivity and selectivity for C_2H_5OH can also be obtained by increasing the activation energy of CH_4 formation by only ~30 kJ mol^{-1}; thus, CH_4 formation can be suppressed, more CH_3 will participate in CH_3CO formation, and more C_2H_5OH will be produced.

According to DFT calculations and microkinetic modeling for ethanol formation from syngas on the Rh/TiO_2 catalyst, the major product is CH_3 rather than CH_3OH during CH_x formation. Thus, starting from CH_3 species, in order to realize high productivity and selectivity for ethanol, the Rh/TiO_2 catalyst requires assistance from a metal promoter, so that more CH_3 species react with CO to form CH_3CO and/or CH_3 hydrogenation to CH_4 is suppressed. Namely, by lowering the activation energy of CH_3CO formation and/or increasing the activation energy of CH_4 formation, CH_4 production can be minimized, so that more CH_3 species contribute to CH_3CO formation, and CH_3CO formation can be maximized, followed by further hydrogenation to ethanol; as a result, the productivity and selectivity for ethanol can be greatly improved.

3.4.2. Function of the promoter. To validate the above predictions, a simple experiment was carried out to examine the effect of Fe, which has been identified as a promoter for ethanol synthesis on a Rh catalyst.[1,5,13,18] To set up the model, a Rh atom from the topmost layer of a Rh_7 nanocluster was

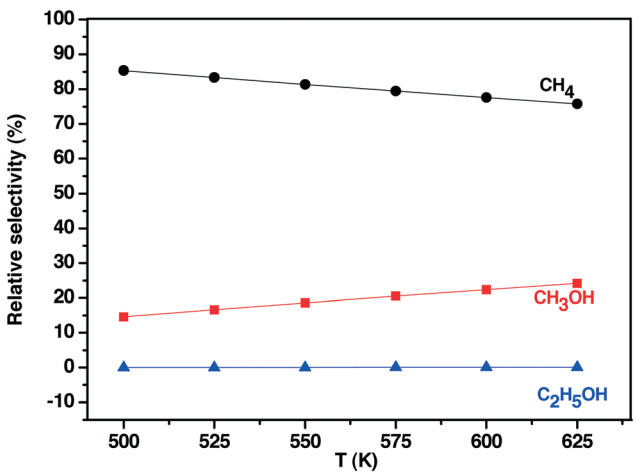

Fig. 6 Temperature dependence of the relative selectivity of the products CH_3OH, CH_4, and C_2H_5OH in syngas conversion on a Rh/TiO_2 model catalyst using the microkinetic modeling technique.

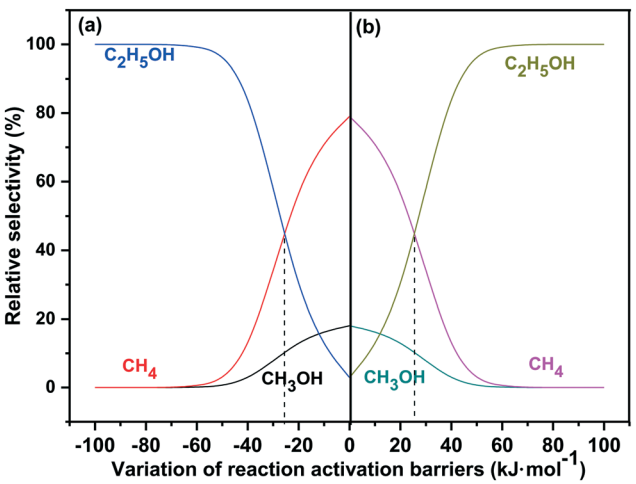

Fig. 7 Effects of the activation energies (E_a) of the reactions (a) CH_3 + CO → CH_3CO and (b) CH_3 + H → CH_4 on the relative selectivity for major products CH_3OH, CH_4, and C_2H_5OH during syngas conversion on Rh/TiO_2 model catalyst using the microkinetic modeling technique.

replaced by an Fe atom, and this was considered as an Fe-promoted Rh/TiO_2 model catalyst ($FeRh_6/TiO_2$); a detailed description of the Fe-promoted Rh/TiO_2 model catalyst is presented in the ESI.†

Our results show that on the Fe-promoted Rh/TiO_2 catalyst, CH_4 formation by CH_3 hydrogenation is exothermic by 21.3 kJ mol^{-1} with an activation energy of 136.6 kJ mol^{-1}, which is 64.2 kJ mol^{-1} higher than that on the Rh/TiO_2 catalyst, suggesting that the Fe promoter can suppress CH_4 production (see Fig. S10†). Interestingly, CO insertion into CH_3 to form CH_3CO on the Fe-promoted Rh/TiO_2 catalyst is exothermic by 69.7 kJ mol^{-1} with a small activation energy of 79.3 kJ mol^{-1}, which 29.4 kJ mol^{-1} lower than that on the Rh/TiO_2 catalyst, indicating that the Fe promoter can promote CH_3CO formation (see Fig. S11†). Thus, on the Rh/TiO_2 catalyst, CH_4 formation is much more favorable than CH_3CO formation, both thermodynamically and dynamically, whereas on the Fe-promoted Rh/TiO_2 catalyst, CH_3CO formation is much more favorable than CH_4 formation, both thermodynamically and dynamically.

According to the microkinetic modeling shown in Fig. 7, the relative selectivities of CH_4 and C_2H_5OH are reversed on increasing the activation energy of CH_4 formation or decreasing the activation energy of CH_3CO formation by only ~30 kJ mol^{-1}; our results show that the activation energy difference between C_2H_5OH and CH_4 formation is about 60 kJ mol^{-1} on the Fe-promoted Rh/TiO_2 catalyst. Namely, introducing an Fe promoter into the Rh/TiO_2 catalyst significantly suppresses CH_4 production and promotes CH_3CO formation, therefore increasing ethanol productivity and selectivity.

3.4.3. Densities of states of Rh_7/TiO_2 and $FeRh_6/TiO_2$ catalysts. It is well known that the reaction barrier of a specific reaction is related to the electronic structure of the catalyst's surface atoms. Hence, a clear insight into the electronic structure effect on the reaction barriers can be gained when the same reaction is compared on different catalysts; the detailed densities of states are presented in the ESI.†

For CH_3 hydrogenation, previous studies[50,107] have investigated CH_4 formation on iron carbides, indicating that a catalyst surface with the d-band center far from the Fermi energy is more active for CH_x hydrogenation. According to our projected densities of states (PDOS) for Rh_7/TiO_2 and $FeRh_6/TiO_2$ catalysts (see Fig. 8), the d-band center of the $FeRh_6/TiO_2$ catalyst is closer to the Fermi level, with a higher d-band energy of −1.70 eV, than that observed for the Rh_7/TiO_2 catalyst with a higher d-band energy of −2.20 eV, indicating that the $FeRh_6/TiO_2$ catalyst is inactive for CH_3 hydrogenation to CH_4 compared to Rh_7/TiO_2; namely, the $FeRh_6/TiO_2$ catalyst is unfavorable for CH_4 formation, which agrees with our kinetic results.

For CO insertion into CH_3, when a CH_3 fragment interacts with CO, and a C–C bond is formed, the doubly occupied 5σ CO orbital interacts with the doubly occupied σ-CH_3 orbital, resulting in doubly occupied bonding and an anti-binding orbital, giving a repulsive interaction. However, the upshift of the d-band center on the $FeRh_6/TiO_2$ catalyst empties more anti-bonding states,[108] which can accept more electrons from CO and CH_3 fragment orbitals than Rh_7/TiO_2 (see Fig. 8), and reduces repulsion, as well as facilitating C–C bond formation. These results are consistent with our DFT calculations showing that the activation energy of CH_4 formation increases, and the activation energy of CH_3CO formation decreases on $FeRh_6/TiO_2$, compared to the corresponding values obtained on Rh_7/TiO_2.

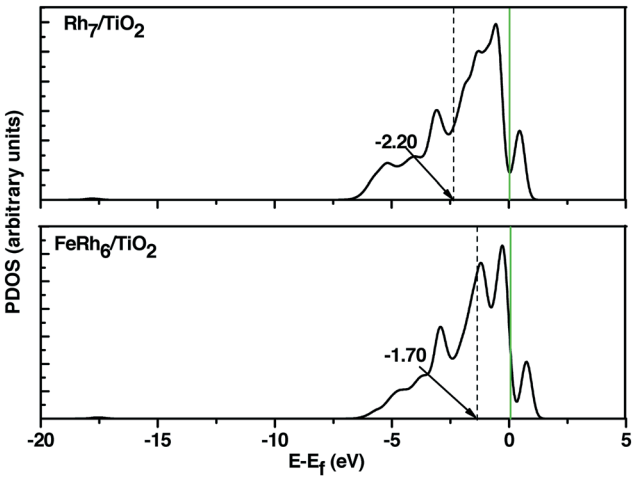

Fig. 8 Projected densities of states (PDOS) for Rh atoms of Rh_7/TiO_2 and $FeRh_6/TiO_2$ model catalysts. The dashed lines represent the location of the corresponding d-band center. The blue lines indicate the Fermi level.

Above analysis about reaction mechanism and densities of states for Fe-promoted Rh/TiO_2 catalyst, we can confirm that the effect of the Fe promoter is very sensitive to CH_4 formation, this is why a wide range of Fe/Rh-ratios were covered in the experiments, which contributes to the suppression of CH_4 production and the promotion of CH_3CO formation. For example, experimental studies[5] found that the addition of Fe_2O_3 greatly suppresses CH_4 production; a catalyst containing 2 wt% Rh and 10 wt% Fe exhibited a maximum ethanol selectivity of about 50%, and a catalyst with an excellent catalytic performance for ethanol contained 2.5% Rh supported on SiO_2 and was promoted by 0.05 wt% Fe.[1] Haider *et al.*[13] have shown that addition of Fe to 2 wt% Rh/TiO_2 improved the selectivity to ethanol, with the highest selectivity being 37% for a sample with 5 wt% Fe. DFT studies by Choi and Liu[18] indicated that an Fe promoter suppresses CH_4 formation in syngas conversion to ethanol on a periodic Rh(111) surface; however, the effect of the Fe promoter on CH_3CO formation has not been mentioned.

3.4.4. The function of the support with respect to ethanol formation. In order to understand the function of the support with respect to ethanol formation, we carried out further comparisons between ethanol formation over a Rh/TiO_2 catalyst with a support and reported studies using a Rh_6 cluster without a support,[52] in which competitive pathways of syngas conversion to C_1 and C_2 oxygenates, such as formaldehyde, methanol, acetic acid, acetaldehyde, and ethanol, were

examined using DFT calculations. Meanwhile, Choi and Liu[18] have investigated syngas conversion to ethanol on a periodic Rh(111) surface.

3.4.4.1. (a) Key intermediate CHO formation with/without support. Previous experiments using the chemical trapping approach have shown the significance of the CHO species for alcohol synthesis on Rh/SiO_2 catalysts,[41] and theoretical studies[18,36,83,103] have also confirmed that ethanol synthesis from syngas is initiated with the key CHO species from CO hydrogenation, and CHO is predominantly responsible for CH_x formation. Thus, CHO formation is the key step in ethanol synthesis from syngas.

For CHO formation, on a Rh_6 cluster without support, Shetty *et al.*[52] have shown that CO hydrogenation to CHO has an activation energy and a reaction energy of 88.0 kJ mol^{-1}, and it is strongly endothermic by 73.0 kJ mol^{-1}. Moreover, on a periodic Rh(111) surface, Choi and Liu[18] have shown that CO hydrogenation to CHO has an activation energy and a reaction energy of 130.3 and 99.4 kJ mol^{-1}, respectively, and that this is the rate-controlling step of the overall conversion. However, in this study, on a Rh_7 cluster supported by TiO_2, CHO formation by CO hydrogenation has an activation energy of only 56.0 kJ mol^{-1}, and this reaction is slightly endothermic by only 3.7 kJ mol^{-1}.

The above results show that on a Rh_6 cluster and a periodic Rh(111) surface without support, CHO formation is highly endothermic, leading to a relatively low surface coverage, which may hinder it from serving as the main reaction channel toward CH_x formation. However, in this study, with a Rh_7 cluster supported by TiO_2, the Rh/TiO_2 catalyst significantly decreases the activation energy and reaction energy of CHO formation; as a result, CHO formation becomes favorable both kinetically and thermodynamically, which makes CHO the predominant channel toward CH_x formation. Moreover, the adsorption energy of the CHO species is 337.7 kJ mol^{-1} over the Rh/TiO_2 catalyst, while it is about 210.0 kJ mol^{-1} on a Rh_6 cluster, suggesting that the Rh/TiO_2 catalyst enhances the stability of CHO intermediates.

Therefore, compared to a Rh_6 cluster and a periodic Rh(111) surface without a support, the TiO_2 support of the Rh/TiO_2 catalyst plays an important role in improving the catalytic activity with CHO formation, promoting CHO formation and further stabilizing the CHO species; as a result, more CHO can be obtained to participate in CH_3 formation; then, CO insertion into CH_3 forms CH_3CO, followed by successive hydrogenation to ethanol.

3.4.4.2. (b) Comparison of favorable CH_x formation with/without support. Previous studies[18,39] have suggested that slow kinetics for CH_x and C_2 oxygenate formation lead to a low yield and poor selectivity for ethanol. Thus, CH_x (x = 1–3) formation plays an important role in ethanol synthesis from syngas.

On a Rh_6 cluster without a support,[52] the most favorable CH_x monomer is the CH_2 species, which is formed *via* the pathway CO + 3H → CHO + 2H → CH_2O + H → CH_2OH → CH_2 + OH; with respect to CO + H, this pathway has an overall activation energy and a reaction energy of 187.0 and 120.0 kJ mol^{-1}, respectively. However, on the Rh/TiO_2 catalyst with support, the most favorable CH_x monomer is the CH_3 species, which is formed *via* the pathway CO + 3H → CHO + 2H → CH_2O + H → CH_3O → CH_3 + O; with respect to CO + H, this pathway has an overall activation energy and a reaction energy of only 85.2 and −30.4 kJ mol^{-1}, respectively.

The above results show that, compared to a Rh_6 cluster without support, the Rh/TiO_2 catalyst with TiO_2 support changes the formation pathway of the CH_x species, further affecting the predominant form of the CH_x species; moreover, the TiO_2 support of the Rh/TiO_2 catalyst exhibits high catalytic activity toward CH_3 formation, which makes the CH_3 species the most favorable CH_x monomer to participate in ethanol formation.

On the other hand, over the Rh/TiO_2 catalyst, CH_3 formation is favorable than CH_3OH formation kinetically; on a Rh_6 cluster, CH_2 formation is also more favorable than CH_3OH formation both thermodynamically and kinetically. However, on the periodic Rh(111) surface,[18] which can be used to model large Rh particle sizes without a support, CH_3OH formation is energetically compatible with CH_3 formation. Therefore, compared to the large Rh cluster size (Rh(111) surface), Rh nanoclusters in both the Rh/TiO_2 catalyst and a Rh_6 cluster exhibit high selectivity for CH_x rather than CH_3OH formation.

3.4.4.3. (c) Comparison of ethanol formation with/without support. Starting from the most favorable CH_x monomer, CH_4 hydrocarbon and C_2 oxygenates can be formed. On a Rh_6 cluster,[52] under hydrogen-rich conditions at normal temperatures and pressures, CH_4 is predominantly formed rather than C_2 oxygenates. On the periodic Rh(111) surface,[18] CH_4 formation by CH_3 hydrogenation is more favorable than CH_3-CO formation by CO insertion into CH_3, and therefore the pure Rh(111) surface is highly selective to CH_4 rather than C_2H_5OH production, which is similar to our present results for the Rh/TiO_2 catalyst with support. Therefore, on the pure Rh catalysts with or without support, the selectivity and productivity of ethanol is controlled by CH_4 production and C–C bond formation between CH_3 and CO.

3.4.5. Implications for ethanol synthesis from syngas on Rh-based catalyst. On the basis of the above discussions, we can confirm that for the Rh/TiO_2 catalyst, the role of the TiO_2 support is to promote the activity and selectivity of CH_3 formation, and suppress CH_3OH production, in which CHO is the key reaction intermediate. Increased CHO formation can produce more CH_3 species, and CHO exists on the catalyst surface under realistic conditions and can be experimentally measured.[99] However, starting from the most favored CH_3 species, CH_4 production is independent of the Rh catalyst support; our results are in agreement with the experimental results, showing that pure Rh catalysts, with or without support, seem to produce only hydrocarbons.[1,13,109,110]

Under realistic conditions, in order to achieve high ethanol productivity and selectivity, the Rh/TiO_2 catalyst requires assistance from a promoter, which should be able to

suppress CH_4 production and/or facilitate C_2 oxygenate formation. According to our calculated results, when introducing a metal promoter M into the Rh/TiO_2 catalyst to form a MRh/TiO_2 catalyst, the promoter M should draw the d-band center of the MRh/TiO_2 catalyst closer to the Fermi level compared to the Rh_7/TiO_2 catalyst; as a result, the MRh/TiO_2 catalyst can suppress CH_4 production and facilitate C_2 oxygenate formation.

Generally speaking, a suitable Rh-based catalyst toward the synthesis of C_2 oxygenates from syngas must include suitable combinations of both a support and a promoter; neither the support nor the promoter alone could achieve the high productivity and selectivity for C_2 oxygenates that has been observed.

Building on DFT calculations and microkinetic modeling, this study can illustrate the functions of the support and promoter in syngas conversion to ethanol on a Rh-based catalyst at a microscopic level, and provide a method of fabricating a more effective Rh-based catalyst. However, in view of the limitations of the simple $Rh_7/TiO_2(110)$ model catalyst, this study gives only qualitative information about the function of the support and promoter. Extensive studies on the fabrication of a more effective Rh-based catalyst should probe into other combinations of supports and promoters, using a larger cluster size for ethanol formation from syngas.

4. Conclusions

Periodic DFT calculations and microkinetic modeling have been performed to investigate ethanol formation from syngas on a Rh/TiO_2 catalyst. Meanwhile, comparisons of ethanol synthesis over Rh/TiO_2, a pure Rh_6 cluster, and a periodic Rh(111) surface, as well as an Fe-promoted Rh/TiO_2 catalyst, have been carried out to determine the functions of the support and promoter. The following results were obtained:

Ethanol, methanol and methane are involved in the process of syngas conversion; compared to pure Rh catalysts without a support, the Rh/TiO_2 catalyst with support can exhibit good catalytic activity and selectivity toward CH_3 rather than CH_3OH formation, and provide more CH_x species for C_2 oxygenate formation; moreover, the Rh/TiO_2 catalyst can stabilizes the key CHO intermediate to promote CH_3 formation. Namely, compared to the pure Rh catalysts without support, the role of the TiO_2 support in the Rh/TiO_2 catalyst is to promote the activity and selectivity of CH_3 formation, suppress CH_3OH production, and provide more CH_3 species for C_2 oxygenate formation. However, CH_4 production from the most favorable CH_3 species is independent of the support on a pure Rh catalyst.

The productivity and selectivity of ethanol synthesis on the Rh/TiO_2 catalyst is determined only by CH_4 formation. In order to achieve high productivity and selectivity for ethanol, the Rh/TiO_2 catalyst requires assistance from promoters to suppress CH_4 production and/or facilitate ethanol formation; introducing an Fe promoter into the Rh/TiO_2 catalyst can effectively suppress CH_4 production and promote ethanol formation, which significantly increases ethanol productivity and selectivity over the Fe-promoted Rh/TiO_2 catalyst, which is a promising candidate for an improved catalyst for ethanol synthesis from syngas. Thus, a suitable Rh-based catalyst toward the synthesis of C_2 oxygenates from syngas should contain a suitable combination of both a support and a promoter.

Finally, the information obtained regarding the function of the TiO_2 support and Fe promoter in the catalytic selectivity of the Rh-based catalyst at the atomic level can potentially be used to develop and design superior Rh-based catalysts for ethanol synthesis from syngas; further studies will consider probing into other combinations of more effective supports (such as a hydroxylated TiO_2 surface and an SiO_2 surface) and other metal promoters.

Acknowledgements

This work is financially supported by the National Natural Science Foundation of China (No. 21476155, 21276003 and 21276171), the Natural Science Foundation of Shanxi Province (No. 2014011012-2), the Program for the Top Young Academic Leaders of Higher Learning Institutions of Shanxi, and the Top Young Innovative Talents of Shanxi.

References

1 V. Subramani and S. K. Gangwal, *Energy Fuels*, 2008, **228**, 14–839.
2 M. M. Bhasin and G. L. O'Connor, Procede preparation selective de derives hydrocarbons oxygenes a deux atoms de carbone. *Belgian Pat.* 824822, 1975, to Union Carbide Corporation.
3 H. Arakawa, K. Takeuchi, T. Matsuzaki and Y. Sugi, *Chem. Lett.*, 1984, **13**, 1607–1610.
4 S. C. C. Steven, S. Girish and A. B. Mark, *Energy Fuels*, 1996, **10**, 524–530.
5 R. Burch and M. J. Hayes, *J. Catal.*, 1997, **165**, 249–261.
6 B. J. Kip, P. A. T. Smeets, J. H. M. C. van Wolput, H. W. Zandbergen, J. van Grondelle and R. Prins, *Appl. Catal.*, 1987, **33**, 157–180.
7 D. H. Mei, R. Rousseau, S. M. Kathmann, V. A. Glezakou, M. H. Engelhard, W. L. Jiang, C. M. Wang, M. A. Gerber, J. F. White and D. J. Stevens, *J. Catal.*, 2010, **27**, 1325–1342.
8 J. L. Hu, Y. Wang, C. S. Cao, D. C. Elliott, D. J. Stevens and J. F. White, *Catal. Today*, 2007, **120**, 90–95.
9 K. G. Fang, D. B. Li, M. G. Lin, M. L. Xiang, W. Wei and Y. H. Sun, *Catal. Today*, 2009, **147**, 133–138.
10 X. H. Mo, J. Gao, N. Umnajkaseam and J. G. Goodwin Jr, *J. Catal.*, 2009, **267**, 167–176.
11 M. Gupta, M. L. Smith and J. J. Spivey, *ACS Catal.*, 2011, **1**, 641–656.
12 J. J. Spivey and A. Egbebi, *Chem. Soc. Rev.*, 2007, **36**, 1514–1528.
13 M. A. Haider, M. R. Gogate and R. J. Davis, *J. Catal.*, 2009, **26**, 9–16.

14 N. D. Subramanian, J. Gao, X. H. Mo, J. G. Goodwin Jr, W. Torres and J. J. Spivey, *J. Catal.*, 2010, **272**, 204–209.
15 H. Ngo, Y. Y. Liu and K. Murata, *React. Kinet., Mech. Catal.*, 2011, **102**, 425–435.
16 L. P. Han, D. S. Mao, J. Yu, Q. S. Guo and G. Z. Lu, *Catal. Commun.*, 2012, **23**, 20–24.
17 Z. L. Fan, W. Chen, X. L. Pan and X. H. Bao, *Catal. Today*, 2009, **147**, 86–93.
18 Y. M. Choi and P. Liu, *J. Am. Chem. Soc.*, 2009, **131**, 13054–13061.
19 M. Ichikawa and T. Fukushima, *J. Chem. Soc., Chem. Commun.*, 1985, 321–323.
20 A. Takeuchi and J. R. Katzer, *J. Phys. Chem.*, 1982, **86**, 2438–2441.
21 S. S. C. Chuang, R. W. Stevens Jr and R. Khatri, *Top. Catal.*, 2005, **32**, 225–232.
22 H. Y. Luo, P. Z. Lin, S. B. Xie, H. W. Zhou, C. H. Xu, S. Y. Huang, L. W. Lin, D. B. Liang, P. L. Yin and Q. Xin, *J. Mol. Catal. A: Chem.*, 1997, **122**, 115–123.
23 S. C. Chuang, J. G. Goodwin Jr and I. Wender, *J. Catal.*, 1985, **95**, 435–446.
24 W. M. Chen, Y. J. Ding, H. Y. Luo, L. Yan, T. Wang, Z. D. Pan and H. J. Zhu, *Chin. J. Appl. Chem.*, 2005, **22**, 470–474.
25 R. P. Underwood and A. T. Bell, *J. Catal.*, 1988, **109**, 61–75.
26 H. Y. Luo, W. Zhang, H. W. Zhou, S. Y. Huang, P. Z. Lin, Y. J. Ding and L. W. Lin, *Appl. Catal., A*, 2001, **214**, 161–166.
27 J. X. H. Gao, A. C. Y. Mo, C. W. Torres and J. G. Goodwin Jr, *J. Catal.*, 2009, **262**, 119–126.
28 R. Burch and M. I. Petch, *Appl. Catal., A*, 1992, **88**, 39–60.
29 H. M. Yin, Y. J. Ding, H. Y. Luo, H. J. Zhu, D. P. He, J. M. Xiong and L. W. Lin, *Appl. Catal., A*, 2003, **243**, 155–164.
30 T. P. Wilson, P. H. Kasai and P. C. Ellgen, *J. Catal.*, 1981, **69**, 193–201.
31 I. Masaru, *Bull. Chem. Soc. Jpn.*, 1978, **51**, 2268–2272.
32 X. D. Xu, E. B. M. Doesburg and J. J. F. Scholten, *Catal. Today*, 1987, **2**, 125–170.
33 J. R. Katzer, A. W. Sleight, P. Gajardo, J. B. Michel, E. F. Gleason and S. McMillan, *Faraday Discuss. Chem. Soc.*, 1981, **72**, 121–133.
34 A. Erdöhelyi and F. Solymosi, *J. Catal.*, 1983, **84**, 446–460.
35 H. Arakawa, T. Fukushima, M. Ichikawa, S. Natsushita, K. Takeuchi, T. Matsuzaki and Y. Sugi, *Chem. Lett.*, 1985, **14**, 881–884.
36 A. Deluzarche, J. P. Hindermann, R. Kieffer, R. Breault and A. Kiennernann, *J. Phys. Chem.*, 1984, **88**, 4993–4995.
37 G. R. Jenness and J. R. Schmidt, *ACS Catal.*, 2013, **3**, 2881–2890.
38 C. M. Li, J. M. Liu and W. Gao, *Catal. Lett.*, 2013, **143**, 1247–1254.
39 R. G. Zhang, G. R. Wang and B. J. Wang, *J. Catal.*, 2013, **305**, 238–255.
40 Y. H. Zhao, M. M. Yang, D. P. Sun, H. Y. Su, K. J. Sun, X. F. Ma, X. H. Bao and W. X. Li, *J. Phys. Chem. C*, 2011, **115**, 18247–18256.
41 Y. H. Zhao, K. J. Sun, X. F. Ma, J. X. Liu, D. P. Sun, H. Y. Su and W. X. Li, *Angew. Chem., Int. Ed.*, 2011, **50**, 5335–5338.
42 X. B. Zheng and A. T. Bell, *J. Phys. Chem. C*, 2008, **112**, 5043–5047.
43 Y. X. Pan, C. J. Liu and Q. F. Ge, *J. Catal.*, 2010, **272**, 227–234.
44 M. Neurock, *J. Catal.*, 2003, **216**, 73–88.
45 F. Y. Li, D. E. Jiang, X. C. Zeng and Z. F. Chen, *Nanoscale*, 2012, **4**, 1123–1129.
46 R. T. Carr, M. Neurock and E. Iglesia, *J. Catal.*, 2011, **278**, 78–93.
47 D. H. Mei, M. Neurock and C. Michael Smith, *J. Catal.*, 2009, **268**, 181–195.
48 Y. H. Chin, C. Buda, M. Neurock and E. Iglesia, *J. Catal.*, 2011, **283**, 10–24.
49 Z. P. Liu and P. J. Hu, *J. Am. Chem. Soc.*, 2003, **125**, 1958–1967.
50 C. F. Huo, Y. W. Li, J. G. Wang and H. J. Jiao, *J. Am. Chem. Soc.*, 2009, **131**, 14713–14721.
51 M. Saeys, M. F. Reyniers, J. W. Thybaut, M. Neurock and G. B. Marin, *J. Catal.*, 2005, **236**, 129–138.
52 S. Shetty, R. A. van Santen, P. A. Stevens and S. Raman, *J. Mol. Catal. A: Chem.*, 2010, **330**, 73–87.
53 Z. B. Ma, Q. Guo, X. C. Mao, Z. F. Ren, X. Wang, C. B. Xu, W. S. Yang, D. X. Dai, C. Y. Zhou, H. J. Fan and X. M. Yang, *J. Phys. Chem. C*, 2013, **117**, 10336–10344.
54 G. R. Bamwenda, S. Tsubota, T. Nakamura and M. Haruta, *J. Photochem. Photobiol., A*, 1995, **89**, 177–189.
55 C. B. Xu, W. S. Yang, Q. Guo, D. X. Dai, M. D. Chen and X. M. Yang, *J. Am. Chem. Soc.*, 2013, **135**, 10206–10209.
56 J. Llorca, N. Homs, J. Sales and P. R. de la Piscina, *J. Catal.*, 2002, **209**, 306–317.
57 N. Strataki, M. Antoniadou, V. Dracopoulos and P. Lianos, *Catal. Today*, 2010, **151**, 53–57.
58 M. Murdoch, G. I. N. Waterhouse, M. A. Nadeem, J. B. Metson, M. A. Keane, R. F. Howe, J. Llorca and H. Idriss, *Nat. Chem.*, 2011, **3**, 489–492.
59 M. A. Nadeem, M. Murdoch, G. I. N. Waterhouse, J. B. Metson, M. A. Keane, J. Llorca and H. Idriss, *J. Photochem. Photobiol., A*, 2010, **216**, 250–255.
60 T. R. Esch, I. Gadaczek and T. Bredow, *Appl. Surf. Sci.*, 2014, **288**, 275–287.
61 J. Zhu, J. X. Yu, Y. J. Wang, X. R. Chen and F. Q. Jing, *Chin. Phys. B*, 2008, **17**, 2216–2221.
62 H. Onishi and Y. Iwasawa, *Chem. Phys. Lett.*, 1994, **226**, 111–114.
63 G. D. Parfitt, The Surface of Titanium Dioxide, *J. Photochem. Photobiol., A*, 1976, **11**, 181–226.
64 H. Shi, Y. C. Liu, M. Miao, T. Wu and Q. Wang, *Chem. Phys. Lett.*, 2013, **584**, 98–102.
65 R. Sánchez de Armas, J. Oviedo, M. A. San Miguel and J. F. Sanz, *J. Phys. Chem. C*, 2007, **111**, 10023–10028.
66 Q. Guo, C. B. Xu, Z. F. Ren, W. S. Yang, Z. B. Ma, D. X. Dai and H. J. Fan, *J. Am. Chem. Soc.*, 2012, **134**, 13366–13373.
67 J. Oviedo, R. Sánchez-de-Armas, M. Ángel San Miguel and J. F. Sanz, *J. Phys. Chem. C*, 2008, **112**, 17737–17740.
68 J. N. Muir, Y. Choi and H. Idriss, *Phys. Chem. Chem. Phys.*, 2012, **14**, 11910–11919.

69 S. Fernandez, A. Markovits and C. Miont, *J. Phys. Chem. C*, 2008, **112**, 14010–14014.
70 X. J. Zou, K. N. Ding, Y. F. Zhang and J. Q. Li, *Int. J. Quantum Chem.*, 2011, **111**, 915–922.
71 J. Zhu, H. Jin, W. J. Chen, Y. Li, Y. F. Zhang, L. X. Ning, X. Huang, K. N. Ding and W. K. Chen, *J. Phys. Chem. C*, 2009, **113**, 17509–17517.
72 A. S. Mazheika, V. E. Matulis and O. A. Ivashkevich, *J. Mol. Struct.*, 2009, **909**, 75–78.
73 Q. S. Zeng, W. K. Chen, W. X. Dai, Y. F. Zhang, Y. Li and X. Guo, *Chin. J. Catal.*, 2010, **31**, 423–428.
74 G. A. Somorjai and C. Aliaga, *Langmuir*, 2010, **26**, 16190–16203.
75 R. A. van Santen, *Acc. Chem. Res.*, 2008, **42**, 57–66.
76 R. A. van Santen, M. Neurock and S. G. Shetty, *Chem. Rev.*, 2010, **110**, 2005–2048.
77 D. A. J. M. Ligthart, R. A. van Santen and E. J. M. Hensen, *J. Catal.*, 2011, **280**, 206–220.
78 V. Schwartz, A. Campos, A. Egbebi, J. J. Spivey and S. H. Overbury, *ACS Catal.*, 2011, **1**, 1298–1306.
79 A. M. Beale and B. M. Weckhuysen, *Phys. Chem. Chem. Phys.*, 2010, **12**, 5562–5574.
80 A. D. Logan, E. J. Braunschweig, A. K. Datye and D. J. Smith, *Langmuir*, 1988, **4**, 827–830.
81 H. Guan, J. Lin, B. Qiao, X. Yang, L. Li, S. Miao, J. Liu, A. Wang, X. Wang and T. Zhang, *Angew. Chem., Int. Ed.*, 2016, **5**, 2820–2824.
82 W. Q. Tian, M. F. Ge, B. R. Sahu, D. X. Wang, T. Yamada and S. Mashiko, *J. Phys. Chem. A*, 2004, **108**, 3806–3812.
83 N. Kapur, J. Hyun, B. Shan, J. B. Nicholas and K. Cho, *J. Phys. Chem. C*, 2010, **114**, 10171–10182.
84 J. C. Wang, Z. X. Liu, R. G. Zhang and B. J. Wang, *J. Phys. Chem. C*, 2014, **118**, 22691–22701.
85 G. Kresse and J. Hafner, *Phys. Rev. B: Condens. Matter Mater. Phys.*, 1993, **47**, 558–561.
86 G. Kresse and J. Furthmuller, *Phys. Rev. B: Condens. Matter Mater. Phys.*, 1996, **54**, 11169–11186.
87 G. Kresse and J. Furthmuller, *Comput. Mater. Sci.*, 1996, **6**, 15–50.
88 J. P. Perdew, J. A. Chevary, S. H. Vosko, K. A. Jackson, M. R. Pederson, D. J. Singh and C. Fiolhais, *Phys. Rev. B: Condens. Matter Mater. Phys.*, 1992, **46**, 6671–6687.
89 G. Kresse and D. Joubert, *Phys. Rev. B: Condens. Matter Mater. Phys.*, 1999, **59**, 1758–1775.
90 H. J. Monkhorst and J. D. Pack, *Phys. Rev. B: Solid State*, 1976, **13**, 5188–5192.
91 M. Methfessel and A. T. Paxton, *Phys. Rev. B: Condens. Matter Mater. Phys.*, 1989, **40**, 3616–3621.
92 S. L. Dudarev, G. A. Botton, S. Y. Savrasov, C. J. Humphreys and A. P. Sutton, *Phys. Rev. B: Condens. Matter Mater. Phys.*, 1998, **57**, 1505–1509.
93 B. J. Morgan and G. W. Watson, *Surf. Sci.*, 2007, **601**, 5034–5041.
94 D. Sheppard, P. H. Xiao, W. Chemelewski, D. D. Johnson and G. Henkelman, *J. Chem. Phys.*, 2012, **136**, 074103.
95 D. Sheppard, R. Terrell and G. Henkelman, *J. Chem. Phys.*, 2008, **128**, 134106.
96 G. Henkelman and H. Jónsson, *J. Chem. Phys.*, 1999, **111**, 7010–7022.
97 R. A. Olsen, G. J. Kroes, G. Henkelman, A. Arnaldsson and H. Jónsson, *J. Chem. Phys.*, 2004, **121**, 9776–9792.
98 R. G. Zhang, F. Liu, X. J. Zhao, B. J. Wang and L. X. Ling, *J. Phys. Chem. C*, 2015, **119**, 10355–10364.
99 A. Kiennemann, R. Breault, J. P. Hindermann and M. Laurin, *J. Chem. Soc., Faraday Trans.*, 1987, **83**, 2119–2128.
100 G. R. Wang, R. G. Zhang and B. J. Wang, *Appl. Catal., A*, 2013, **466**, 77–89.
101 M. K. Zhuo, A. Borgn and M. Saeys, *J. Catal.*, 2013, **297**, 217–226.
102 X. C. Xu, J. J. Su, P. F. Tian, D. L. Fu, W. W. Dai, W. Mao, W. K. Yuan, J. Xu and Y. F. Han, *J. Phys. Chem. C*, 2015, **119**, 216–227.
103 C. Mazzocchia, P. Gronchi, A. Kaddouri, E. Tempesti, L. Zanderighi and A. Kiennemann, *J. Mol. Catal. A: Chem.*, 2001, **165**, 219–230.
104 P. Liu and J. A. Rodriguez, *J. Chem. Phys.*, 2007, **126**, 164705–164712.
105 P. Liu, A. Logadottir and J. K. Nørskov, *Electrochim. Acta*, 2003, **48**, 3731–3742.
106 X. J. Zhao, R. G. Zhang, Q. Wang, D. B. Li, B. J. Wang and L. X. Ling, *RSC Adv.*, 2014, **4**, 58631–58642.
107 T. H. Pham, Y. Y. Qi, J. Yang, X. Z. Duan, G. Qian, X. G. Zhou, D. Chen and W. K. Yuan, *ACS Catal.*, 2015, **5**, 2203–2208.
108 J. D. Li, E. Croiset and L. Ricardez-Sandoval, *J. Mol. Catal. A: Chem.*, 2012, **365**, 103–114.
109 T. Iizuka, Y. Tanaka and K. Tanabe, *J. Catal.*, 1982, **76**, 1–8.
110 F. Solymosi, I. Tombácz and M. Kocsis, *J. Catal.*, 1982, **75**, 78–93.